JOURNAL OF THERMOPHYSICS AND HEAT TRANSFER
Vol. 20, No. 4, October–December 2006

Simple Deployable Radiator with Autonomous Thermal Control Function

Hosei Nagano* and Yuji Nagasaka†
Keio University, Yokohama, Kanagawa 223-8522, Japan
and
Akira Ohnishi‡
Japan Aerospace Exploration Agency, Sagamihara, Kanagawa 229-8510, Japan

DOI: 10.2514/1.17988

The concept, detailed design, fabrication, and test results of a reversible thermal panel, which is a new, passive, and lightweight 100 W-class deployable radiator with an environment-adaptive function, is described. The reversible thermal panel changes its function reversibly from a radiator to a solar absorber by deploying/stowing the radiator/absorber reversible fin upon changes in the heat dissipation and thermal environment, and is effective for the thermal control of high power density small satellites, landers, and interplanetary spacecrafts. Parametric studies were conducted with detailed simulation models, and the reversible thermal panel configuration that satisfies thermal requirements with the restraints of weight and fin efficiency variation was determined. Based on the analytical results, a reversible thermal panel engineering model was fabricated using high thermal conductivity graphite sheets in the reversible fin and a shape-memory alloy in the passive deployment/stowing actuator. Test results indicated excellent performance of the reversible thermal panel as a passive radiator from the standpoints of heat-rejection capability, specific heat rejection, and variation of the fin efficiency. The effectiveness of the reversible thermal panel as a solar absorber that can be substituted for a survival heater was also demonstrated.

Nomenclature

A_{BP}	=	base plate area
A_{RAD}	=	radiator area
A_{RF}	=	fin area
A_{RTP}	=	reversible thermal panel total area
d_{BP}, d_F	=	thickness of base plate and fin, respectively
E_R	=	radiation parameter
F	=	view factor
G_1	=	aspect ratio of reversible thermal panel
l_0	=	length of equipment in the x direction
l_1	=	length of base plate in the x direction
M_{RTP}	=	reversible thermal panel total weight
Q_L	=	heat load
Q_{RAD}	=	heat rejection
R_C	=	thermal resistance parameter
T_{HS}	=	heat source temperature
T_O, T_C	=	open and close temperature, respectively
T_S	=	sink temperature
T_U, T_L	=	upper and lower limit temperature, respectively
u, v	=	margins for bend and bolts, respectively
w_0	=	width of equipment in the y direction
w_1	=	width of base plate in the y direction
x, y	=	Cartesian coordinates
X, Y	=	dimensionless coordinates
α_S	=	solar absorptance
β	=	geometric parameter
ε_H	=	total hemispherical emittance
ε_{ABS}, ε_{RAD}	=	total hemispherical emittance of absorber and radiator surface, respectively
σ	=	Stefan–Boltzmann constant
θ	=	angle
η_F	=	radiator fin efficiency
Ω	=	dimensionless heat dissipation
Θ	=	dimensionless temperature
λ_{xy}	=	in-plane thermal conductivity

Presented as Paper 5073 at the 38th AIAA Thermophysics Conference, Westin Harbour Castle Toronto, Ontario, Canada, 6–9 June 2005; received 13 September 2005; revision received 1 November 2005; accepted for publication 1 November 2005. Copyright © 2005 by the American Institute of Aeronautics and Astronautics, Inc. All rights reserved. Copies of this paper may be made for personal or internal use, on condition that the copier pay the $10.00 per-copy fee to the Copyright Clearance Center, Inc., 222 Rosewood Drive, Danvers, MA 01923; include the code $10.00 in correspondence with the CCC.

*Postdoctoral Fellow, Department of Mechanical Engineering, 3-14-1 Hiyoshi, Yokohama, Kanagawa 223-8522. Member AIAA.
†Professor, Department of System Design Engineering, 3-14-1 Hiyoshi, Yokohama, Kanagawa 223-8522.
‡Assistant Professor, Institute of Space and Astronautics Science, 3-1-1 Yoshinodai, Sagamihara, Kanagawa 229-8510.

I. Introduction

IT is essential to develop advanced thermal control techniques that satisfy strict thermal requirements in order to enable future spacecrafts. In small satellites or microsatellites, as power-to-external area ratios increase through the use of high-density electronic packing, the spacecraft bus does not have enough area to reject the internally generated waste heat. Interplanetary probes and landers are exposed to a wide variety of thermal environments because the heat generated as a result of solar flux will vary with the distance from the sun, and the range of the temperature excursion of the day-night cycle is extremely large. In particular, Japanese missions that do not use radioisotope technology require original energy-saving methodologies. Conventionally, heat pipes and thermal louvers have been used as heat transport and temperature control devices, respectively. Their use is a proven standard and reliable approach, but their adoption in future missions has limitations in terms of weight and performance.

Recently, deployable radiators with fluid loops have been investigated, and some have been applied on spacecrafts [1,2]. The use of a deployable radiator is effective in spacecraft that lack sufficient area for radiators; however, it is limited to applications on large satellites, due to the weight and complicated construction of such radiators, and to the need for large heater power under cold case. Variable emittance coatings (VECs), such as thermochromic materials, electrochromic materials and microelectro mechanical systems (MEMS) louvers, have also been investigated as new thermal control devices that can be substituted for a thermal louver [3–5]. Thermochromic variable emittance devices, whose emittance varies from 0.3 to 0.7, have been developed, and one such device was used on the Japanese asteroid

explorer Hayabusa, which was launched in 2003 [6]. VECs are lightweight and simple, and present great promise, but when they are applied to a large radiator area, the amount of heat dissipation, which is in proportion to both the emittance and the area, becomes relatively large even under low-emittance conditions. The variable-area radiator is another approach, based on the use of phase-change phenomena, and has been studied since the 1970s [7,8]. However, it has not been put to practical use due to its technologically complicated mechanism.

In the present study, a new, passive, and lightweight 100 W-class deployable radiator with autonomous thermal control function is proposed in order to satisfy the various thermal requirements mentioned previously. This autonomous device, the reversible thermal panel, consists of a base plate, a rotary actuator, and flexible high thermal conductivity materials, which are used for heat transport from a heat source to the tip of a deployable fin. The RTP is a conductive deployable radiator that allows for the optional addition of dual functions, one of which changes the radiator fin angle according to the inner temperature of the spacecraft, and the other serves as a solar absorber that absorbs solar energy for heat retention of electronics. A preliminary conceptual design of the RTP was investigated, and a breadboard model (BBM) was defined, fabricated, and tested, demonstrating the effectiveness of the RTP [9,10]. Additionally, a commercially developed pyrolytic graphite sheet (PGS), having the characteristics of high thermal conductivity, light weight, and good flexibility, has been proposed as the flexible high thermal conductive materials of the RTP, and its thermophysical properties including thermal conductivity, total hemispherical emittance, and solar absorptance were evaluated [10–12].

This paper describes the concept and detailed design of the reversible thermal panel. Parametric studies were conducted with detailed simulation models in order to determine the appropriate RTP configuration to satisfy thermal requirements within the restraints of weight and fin efficiency variation. An RTP engineering model (EM) was fabricated and tested based on the detailed design. The test results indicated excellent performance of the RTP as a passive radiator from the standpoint of heat-rejection capability, specific heat rejection, and variation of the radiator fin efficiency; the effectiveness of the RTP as a solar absorber that can be substituted for a survival heater was also shown. Additionally, feasibility of the RTP concept was demonstrated using the RTP EM equipped with a rotary actuator breadboard model, which was manufactured with a shape-memory alloy (SMA).

II. Concept and Thermal Characteristics of the Reversible Thermal Panel

A. Concept of the Reversible Thermal Panel

Figure 1 shows a simple conceptual and a cross-sectional schematic view of the RTP. The RTP is composed of a base plate, heat transport units, and a passive reversible rotary actuator (RRA). The heat source is attached to the base plate, the rear side of which is used as a radiator. The heat transport units are composed of a thermal doubler, which is set between the base plate and the heat source, a radiator/absorber reversible fin, which is exposed to the space environment, and heat transport paths, which exchange heat between the thermal doubler and the radiator/absorber reversible fin. The thermooptical characteristics of the radiator side of the radiator/absorber reversible fin are the reverse of the characteristics of the absorber side. The radiator side has a low α_S/ε_H value, whereas the absorber side has a high α_S/ε_H value. By deploying/stowing the radiator/absorber reversible fin under different temperature conditions of the heat source, the RTP changes its function reversibly from radiator to solar absorber. The fin positions are controlled by the passive RRA, which is thermally coupled to the heat source but is protected and isolated from the external environment by a housing cover. When the heat source temperature increases, the rise in temperature within the housing warms the actuator, which then generates thermal torques that rotate the reversible fin toward its deployed position, leading to an increase in radiation to space. As the temperature decreases, the actuator moves the reversible fin toward its stowed position, completely covering the surface of the base plate radiator with the radiator side of the reversible fin, and blocking more of the radiator's exposure to space. In addition, if solar irradiation is available, solar power is absorbed and used as a heat source for a survival heater. That is, the RTP absorber surface absorbs the sunlight and converts it into heat that is transported into the heat source and warms it. This autonomous deployment and stowing of the reversible fin maintains acceptable temperatures by compensating for changes in dissipation and environment heating.

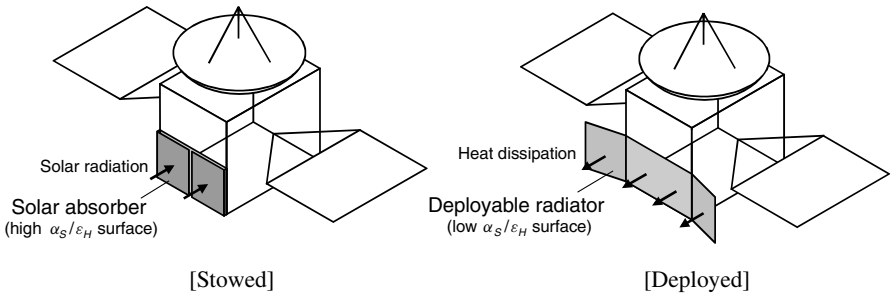

a) Simple conceptual view

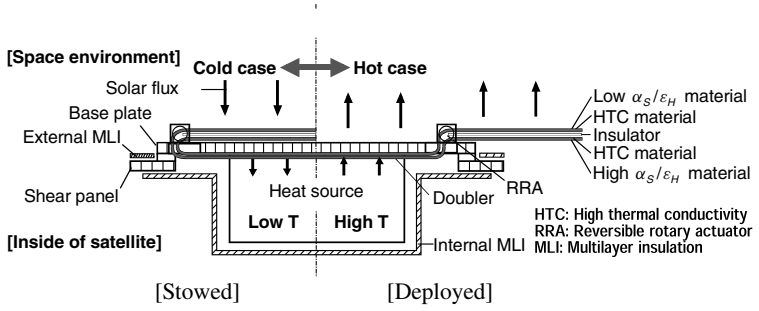

b) Cross-sectional view

Fig. 1 Schematic views of the reversible thermal panel.

The RTP proposed here is an ultimately autonomous thermal control device. However, by adding or reducing the frequency of deployment and rear surface properties, the RTP can be adapted to various thermal requirements and environments such as the following:

1) 100 W-class one-way deployable radiator with low α_S/ε_H value on the rear side of the reversible fin for high heat dissipation. Applicable to small satellites or microsatellites with simple orbits.

2) Reversibly deployable/stowable radiator with insulation on the rear side of the reversible fin for nonheat exchange or/and for protection of the radiator surface from contamination. Applicable to landers such as those for a lunar base.

3) Reversibly deployable/stowable radiator with a high α_S/ε_H value or VEC on the rear surface of the reversible fin for solar absorption or/and for wider heat dissipation change under conditions between hot case (deployed) and cold case (stowed). Applicable to interplanetary probes.

Additionally, the number of wings (single or dual), and the deployment/stowing reversible mechanism (SMA, bimetal, paraffin actuator, or motor control with electric power) can also be selected for optimum performance.

B. Basic Thermal Characteristics of RTP

Figure 2 shows an RTP analytical model, which is a quarter-symmetry model that accounted for the symmetry of the RTP. The dimensions of the RTP were $2l_1 + u$ in length, $w_1 + v$ in width, and the RTP was divided into three parts, a base plate area, a radiator/absorber fin area, and margins for bolts and for bending. In addition, the radiator fin and absorber fin were thermally insulated in the thickness direction. The total hemispherical emittance of the surfaces of the base plate and radiator fin was $\varepsilon_{\mathrm{RAD}}$ whereas that of absorber fin alone was $\varepsilon_{\mathrm{ABS}}$. The absolute temperature of the heat source and the deep space were T_{HS} and T_{S}, respectively. This model was based on the following assumptions:

1) The heat exchange by radiation and conduction occurs only among RTP components (base plate, radiator fin, and absorber fin) and the space environment; there is no heat exchange between the RTP and other structures of the spacecraft. There is no external heat input from the environment except for background radiation.

2) When the fin is entirely stowed and only the absorber surface is exposed, the surface of radiator fin and base plate are entirely covered by each other, and heat exchange to the space is performed only by the absorber surface.

3) The absorber surface is continuously exposed to the space environment irrelevant to the fin position.

4) The thickness d_F of the RTP is far smaller than length $2l_1$ and width w_1.

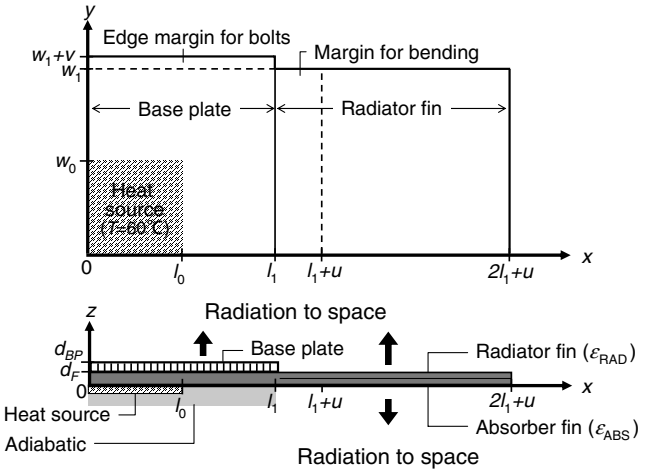

Fig. 2 RTP analytical model.

1. Heat-Rejection Performance when the Thermal Conductivity is Infinite

Assuming that the in-plane thermal conductivity λ_{xy} is infinite, $u = v = 0$, $d_{\mathrm{BP}} = 0$, and there is no contact heat resistance between the base plate and heat source, the total heat rejection $Q_{\mathrm{RAD}(\theta)}$ of the RTP at an arbitrary fin angle θ is expressed by this simple equation

$$Q_{\mathrm{RAD}(\theta)} = \left[\frac{2\varepsilon_{\mathrm{RAD}}F_{\mathrm{BS}}(\theta)}{F_{\mathrm{BS}}(\theta)(1-\varepsilon_{\mathrm{RAD}})+\varepsilon_{\mathrm{RAD}}} + \varepsilon_{\mathrm{ABS}}\right]\cdot\sigma A_{\mathrm{RAD}}(T_{\mathrm{HS}}^4 - T_S^4) \tag{1}$$

where $F_{\mathrm{BS}}(\theta)$ is a view factor of the base plate against the space environment at the arbitrary deployment fin angle θ; when $\theta = 180$ deg, the view factor is $F_{\mathrm{BS}} = 1$ and the total heat rejection $Q_{\mathrm{RAD}(180\,\mathrm{deg})}$ reaches its maximum. When dimensionless heat rejection is defined by this equation

$$\Omega_{\mathrm{RAD}(\theta)} = Q_{\mathrm{RAD}(\theta)}/Q_{\mathrm{RAD}(180\,\mathrm{deg})} \tag{2}$$

Eq. (1) can be transformed to be

$$\Omega_{\mathrm{RAD}(\theta)} = \frac{2\varepsilon_{\mathrm{RAD}}F_{\mathrm{BS}}(\theta) + \varepsilon_{\mathrm{ABS}}[F_{\mathrm{BS}}(\theta)(1-\varepsilon_{\mathrm{RAD}})+\varepsilon_{\mathrm{RAD}}]}{(2\varepsilon_{\mathrm{RAD}}+\varepsilon_{\mathrm{ABS}})[F_{\mathrm{BS}}(\theta)(1-\varepsilon_{\mathrm{RAD}})+\varepsilon_{\mathrm{RAD}}]} \tag{3}$$

From Eq. (3), it is clear that the heat-rejection performance is determined by the total hemispherical emittance of the radiator/absorber fin and the view factor between the RTP surface and the space environment. $R_C = 0$ in Fig. 3 shows dimensionless total heat rejection $\Omega_{\mathrm{RAD}(\theta)}$ in the case of $\gamma = \varepsilon_{\mathrm{RAD}}/\varepsilon_{\mathrm{ABS}} = 3$. From this graph, it was confirmed that the view factor increases to 1.0 as the deployment fin angle increases, and, as a result, heat rejection increases.

Assuming that the fin is entirely deployed ($\theta = 180$ deg) at temperatures higher than T_O, that it is entirely stowed ($\theta = 0$ deg) at temperatures lower than T_C, and that, between $T_C \le T_{\mathrm{HS}} \le T_O$, the temperature T_{HS} is a one-dimensional function of the view factor $F_{\mathrm{BS}}(\theta)$, the RTP steady heat rejection at an arbitrary temperature is expressed by the following equations:

$$\Omega_{\mathrm{RAD}} = \frac{\varepsilon_{\mathrm{ABS}}}{2\varepsilon_{\mathrm{RAD}}+\varepsilon_{\mathrm{ABS}}}\cdot\frac{(\Theta_{\mathrm{HS}}+\Theta_L)^4 - \Theta_S^4}{(1+\Theta_L)^4 - \Theta_S^4} \quad \text{at } \Theta_{\mathrm{HS}} \le \Theta_C \tag{4}$$

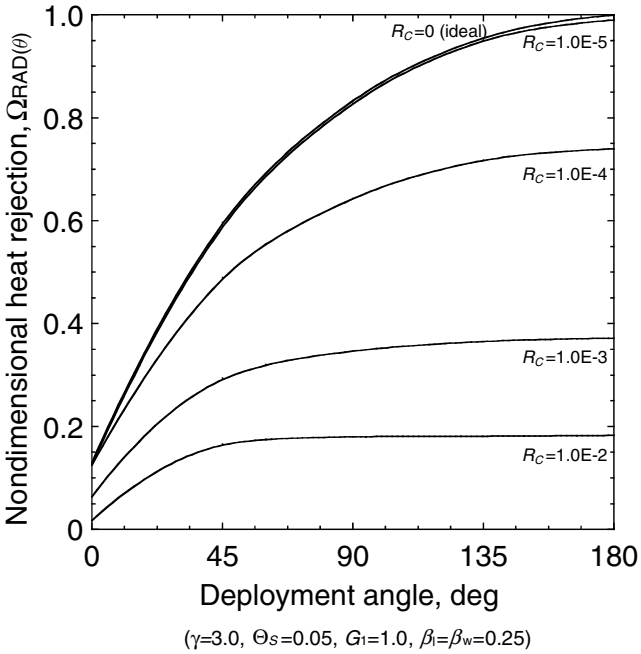

Fig. 3 Deployment angle dependence of heat rejection for RTP.

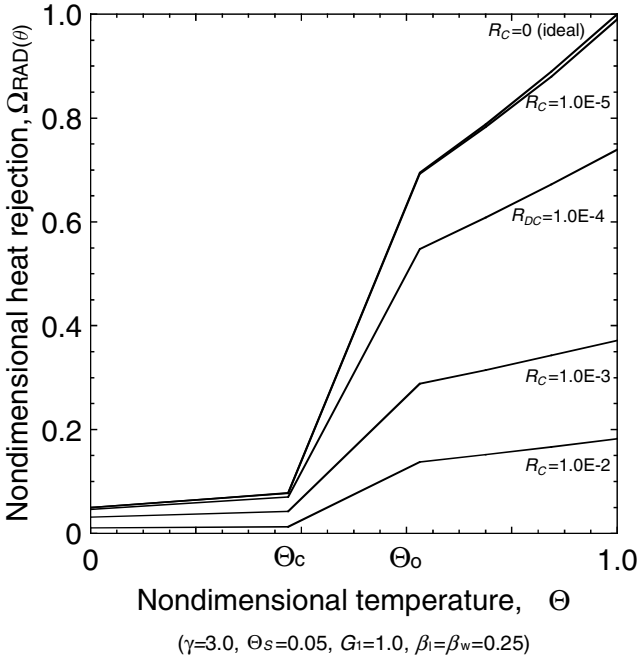

Fig. 4 Temperature dependence of heat rejection for RTP.

$$\Omega_{\mathrm{RAD}} = \left\{1 - \frac{2\varepsilon_{\mathrm{RAD}}}{2\varepsilon_{\mathrm{RAD}} + \varepsilon_{\mathrm{ABS}}} \cdot \frac{\Theta_O - (\Theta_{\mathrm{HS}} + \Theta_L)}{\Theta_O - \Theta_C}\right\} \times \frac{(\Theta_{\mathrm{HS}} + \Theta_L)^4 - \Theta_S^4}{(1 + \Theta_L)^4 - \Theta_S^4} \quad \text{at } \Theta_C \le \Theta_{\mathrm{HS}} \le \Theta_O \tag{5}$$

$$\Omega_{\mathrm{RAD}} = \frac{(\Theta_{HS} + \Theta_L)^4 - \Theta_S^4}{(1 + \Theta_L)^4 - \Theta_S^4} \quad \text{at } \Theta_{\mathrm{HS}} \ge \Theta_O \tag{6}$$

where

$$\Theta_{\mathrm{HS}} = \frac{T_{\mathrm{HS}} - T_L}{T_U - T_L}, \qquad \Theta_L = \frac{T_L}{T_U - T_L}, \qquad \Theta_S = \frac{T_S}{T_U - T_L}$$
$$\Theta_C = \frac{T_C - T_L}{T_U - T_L}, \quad \text{and} \quad \Theta_O = \frac{T_O - T_L}{T_U - T_L} \tag{7}$$

T_U is the upper limit temperature and T_L is the lower limit temperature. $R_C = 0$ in Fig. 4 shows that the heat-rejection change with heat source temperature can be calculated from Eqs. (4–7). From these results, it is clarified that the RTP has a wide range of heat rejection.

2. Heat-Rejection Prediction Considering the Two-Dimensional Thermal Conductivity in the In-Plane Direction

Next, let us consider the effects of in-plane thermal conductivity λ_{xy} and fin thickness d_F on the heat-rejection performance. The steady-state heat-conduction equation of unit volume $d_F dx dy$ at (x, y) can be expressed as

$$\frac{\partial^2 \Theta}{\partial X^2} + G_1^2 \frac{\partial^2 \Theta}{\partial Y^2} = R_C E_R(X, Y) \tag{8}$$

where

$$X = \frac{x}{l_1}, \qquad Y = \frac{y}{w_1}, \qquad G_1 = \frac{l_1}{w_1} \tag{9}$$

R_C is the thermal resistance parameter and defined by the equation

$$R_C = \frac{\sigma \Delta T_{U-L}^3 l_1^3}{\lambda_{xy} d_F} \tag{10}$$

and $E_R(X, Y)$ is the radiative parameter and defined by the equations

$$E_R(X, Y) = \varepsilon_{\mathrm{RAD}} \left[(\Theta + \Theta_L)^4 - F_{iS}\Theta_S^4 - \frac{1}{\sigma \Delta T_{U-L}} \sum_{j=1}^{n} F_{ij}(\theta) J_j(\theta) \right] \quad \text{at } 0 < X < 1, 0 < Y < 1 \tag{11}$$

and

$$E_R(X, Y) = \varepsilon_{\mathrm{RAD}} \left[(\Theta + \Theta_L)^4 - F_{iS}\Theta_S^4 - \frac{1}{\sigma \Delta T_{U-L}} \sum_{j=1}^{n} F_{ij}(\theta) J_j(\theta) \right] + \varepsilon_{\mathrm{ABS}}[(\Theta + \Theta_L)^4 - \Theta_S^4] \quad \text{at } 1 < X < 2, 0 < Y < 1 \tag{12}$$

F_{iS} is the view factor between an element i and the space environment, and $F_{ij}(\theta)$ is the view factor between an element i and another element j at an angle of θ. $J_j(\theta)$ is the total radiative energy from the element j at a unit area and unit second at an angle of θ. The boundary conditions are as follows:

$$\frac{\partial \Theta}{\partial X} = 0 \quad \text{at } X = 0, X = 2 \tag{13}$$

$$\frac{\partial \Theta}{\partial Y} = 0 \quad \text{at } Y = 0, Y = 1 \tag{14}$$

and

$$\Theta = \Theta_{\mathrm{HS}} \quad \text{at } 0 \le X \le \beta_1, 0 \le Y \le \beta_w \tag{15}$$

where

$$\beta_l = \frac{l_0}{l_1}, \qquad \beta_w = \frac{w_0}{w_1} \tag{16}$$

Using Eqs. (8–16), the temperature dependence and deployment angle dependence of dimensionless heat rejection were numerically obtained. Figures 3 and 4 show the deployment angle dependence and the temperature dependence of heat rejection by changing the thermal resistance parameter R_C from 0 to 1.0, when the analytical conditions are $\gamma = 3.0$, $\Theta = 1.0$, $\Theta_S = 0.05$, $G_1 = 1.0$, and $\beta_l = \beta_w = 0.25$. These results demonstrate that heat-rejection performance and heat-rejection change of the RTP strongly depend on the product of the in-plane thermal conductivity λ_{xy} and fin thickness d_F.

III. Detailed Design and Fabrication of the RTP Engineering Model

A. Detailed Design of the RTP Engineering Model

To design an RTP engineering model, the thermophysical properties of the RTP were fixed, and the effects of variation of the RTP configuration parameters on thermal performance were evaluated by parametric study with the same analytical model shown in Fig. 2. The materials that compose the RTP are almost the same as those composing the RTP breadboard model [9,10]. PGSs are used as the thermal doubler and reversible fin. Silverized polyester imide film (PEI/Ag) is used as a radiator surface because it has a low α_S/ε_H value and high durability against UV irradiation and has been used for radiator surfaces in many Japanese spacecraft. On the absorber side, the optical properties of PGS were used, because PGS has a high α_S/ε_H value. A honeycomb sandwich panel was used as the base plate. The thicknesses of the face sheet (7075T6) and the core of the aluminum honeycomb sandwich panel were 0.3 and 12.7 mm, respectively. The three-dimensional effective thermal conductivities of this panel were calculated based on [13]. Table 1 lists the thermophysical properties of materials with other analysis conditions. The value of thermal contact conductance (TCC) between the base plate

Table 1 Input parameters, constants, and thermophysical properties.

Items	Value
Fin thickness	1.0, 2.0, 4.0 mm
RTP area	0.1–1.3 m^2
RTP aspect ratio	0.2–4.0
PGS thermal conductivity	468 W/mK
Radiator surface	PEI/Ag: $\alpha_S/\varepsilon_H = 0.15/0.82$
Absorber surface	PGS: $\alpha_S/\varepsilon_H = 0.72/0.35$
TCC	1.2×10^{-3} m^2 K/W
Heat source temp.	60°C
Heat source area	0.2×0.2 m^2
Sink temperature	−269°C

and the PGSs was obtained from the test results of the RTP BBM evaluation [10]. The main input variables of the RTP configuration are the RTP size, $A_{\mathrm{RTP}}[=4(2l_1w_1 + uw_1 + vl_1)]$, the fin thickness of the RTP d_F and the aspect ratio of the RTP l_1/w_1. The heat rejection and specific heat rejection, which are obtained by dividing the heat rejection by the RTP total weight, and the variation of the radiator fin efficiency are evaluated as thermal performances by parametric studies. The RTP total weight is the sum of the base plate (face sheets and honeycomb core), the radiator fin (PGS + 25um acrylic adhesive tapes), and two RRAs (assumed to be 100 g). The variation of the radiator fin efficiency by the deployment and stowing of the radiator/absorber fin is expressed by the following equation:

$$\Delta\eta_F = \eta_{F(180\,\mathrm{deg})} - \eta_{F(0\,\mathrm{deg})} \tag{17}$$

The radiator fin efficiency $\eta_{F(\theta)}$ is defined as the ratio of the actual heat rejection to the estimated heat rejection in the case that the entire RTP is at equipment temperature, and can be expressed as

$$\eta_{\mathrm{F}} = \frac{Q_{\mathrm{RAD}(\theta)}}{\varepsilon_{\mathrm{RAD}}\sigma(A_{\mathrm{BP}} + A_{\mathrm{RF}})(T_{\mathrm{HS}}^4 - T_{\mathrm{S}}^4) + \varepsilon_{\mathrm{ABS}}\sigma A_{\mathrm{RF}}(T_{\mathrm{HS}}^4 - T_{\mathrm{S}}^4)} \tag{18}$$

where $Q_{\mathrm{RAD}(\theta)}$ is the actual heat rejection at an arbitrary fin angle. To determine an appropriate RTP EM configuration, the following restraints of weight and fin efficiency variation were determined:

1) The maximum heat-rejection capability, that is, the heat-rejection capability when the reversible fin is deployed, is more than 100 W in the full size model ($Q_{\mathrm{RAD}} \geq 100$ W).

2) The specific heat rejection when the reversible fin is deployed is more than 150 W/kg ($Q_{\mathrm{RAD}}/M_{\mathrm{RTP}} \geq 150$ W/kg).

3) The change in radiator fin efficiency with a change in the reversible fin position from deployed to stowed is approximately 0.4 ($\Delta\eta_F \geq 0.4$).

B. Analytical Results

1. Relationship Between RTP Size and Heat Rejection at a Constant Aspect Ratio

Figure 5 shows the heat rejection Q_{RAD} and the fin efficiency η_F of the RTP with changes in RTP size A_{RTP} and fin thickness d_F when $l_1/w_1 = 1$, $u = 50$ mm, and $v = 20$ mm. It was confirmed that the heat-rejection performance increases as RTP size increases, whereas fin efficiency decreases as RTP size increases. It was also confirmed that the heat-rejection performance and radiator fin efficiency increase as fin thickness increases.

The region that satisfies both a heat-rejection value of more than 100 W and a value of more than 0.4 for variation of the radiator fin efficiency by the deployment and stowing of the fin is $A_{\mathrm{RTP}} \leq 0.36$ m^2 for $d_F = 1$ mm, $A_{\mathrm{RTP}} \leq 0.52$ m^2 for $d_F = 2$ mm, and $A_{\mathrm{RTP}} \leq 0.78$ m^2 for $d_F = 4$ mm.

Figure 6 shows the specific heat rejection $Q_{\mathrm{RAD}}/M_{\mathrm{RTP}}$ with changes in RTP size A_{RTP} and fin thickness d_F when $l_1/w_1 = 1$, $u = 50$ mm, and $v = 20$ mm. It was confirmed that there exists a maximum point of specific heat rejection when the RTP total area is approximately $A_{\mathrm{RTP}} = 0.2$ m^2. It was also confirmed that the specific heat rejection decreases as fin thickness increases, which is the

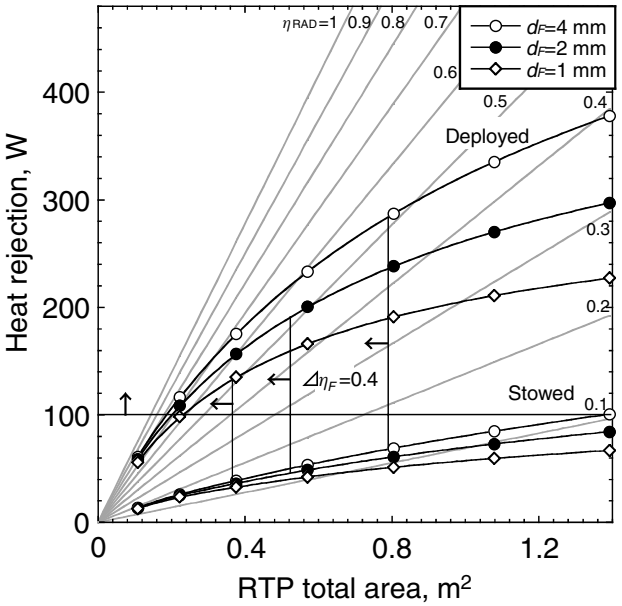

Fig. 5 Relationship between RTP area and heat rejection.

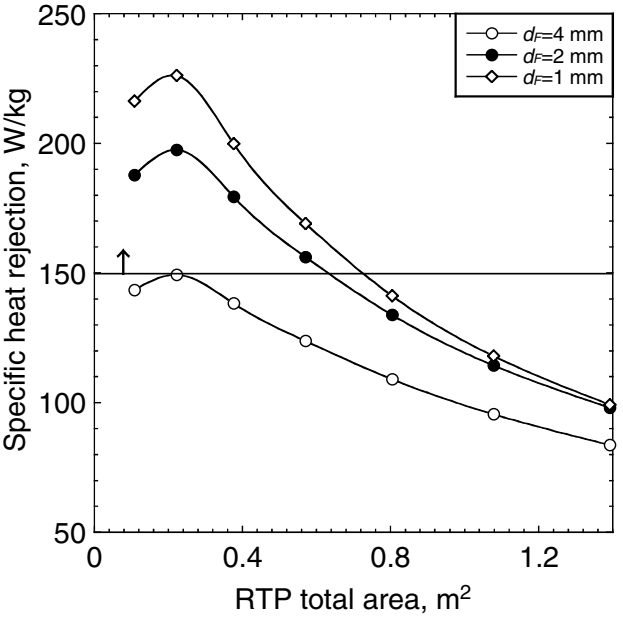

Fig. 6 Relationship between RTP area and specific heat rejection.

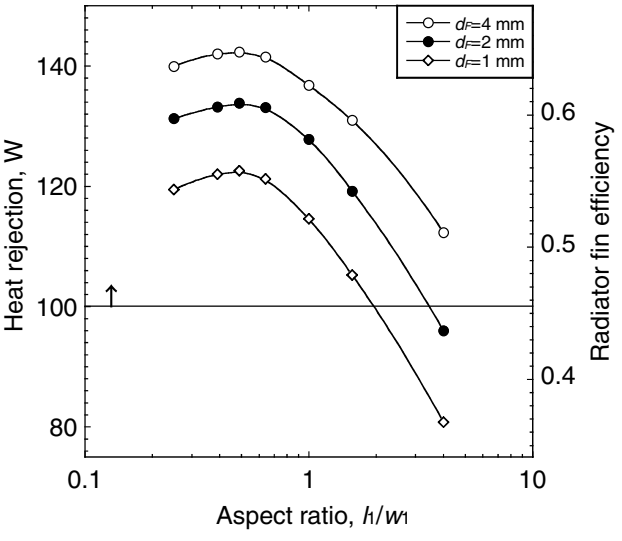

Fig. 7 Relationship between RTP aspect ratio and heat rejection.

Table 2 Design parameters.

Thickness [mm]	RTP area [m^2]	l_1/w_1 Ratio
1.0	0.23–0.36	0.25–1.96
2.0	0.20–0.52	0.25–3.45

Table 3 Specification of RTP engineering model.

RTP component	Material	Size [mm]
Base plate	A7075 T6, (0.3 mm × 2) Al 1/4-5052-0.0015P-t12.7 Ag/PEI (surface) Al/PI (edge)	410 × 200 × t13.3
Radiator fin	PGS (5 pieces) Ag/PEI (surface) Al/PET/Al (rear face)	180 × 500 × t1
Absorber fin	PGS (5 pieces) PGS (surface) Al/PET/Al (rear face)	180 × 500 × t1
Surface finish	Ag/PEI	t0.075
Insulator	Velcro, embossed Mylar	200 × 200 × t3
MLI	Al/PET/Al	10 layer
Thermal dummy	A5052 with constantan wire	180 × 180 × t1
Solar simulator	Sheet heater (3 pieces)	12 × 20
Total weight		0.39 kg

opposite tendency from the case of heat rejection. The area that satisfies a specific heat rejection of more than 150 W/kg is $A_{\mathrm{RTP}} \leq 0.74$ m^2 for $d_F = 1$ mm and $A_{\mathrm{RTP}} \leq 0.64$ m^2 for $d_F = 2$ mm. When the fin thickness is $d_F = 4$ mm, specific heat rejection is always below 150 W/kg.

2. Relationship Between RTP Aspect Ratio and Heat Rejection at a Constant RTP Size

Figure 7 shows the heat rejection Q_{RAD} with changes in the aspect ratio l_1/w_1 and fin thickness d_F when $l_1 \times w_1 = 4.0 \times 10^{-2}$ m^2 and $u = v = 0$ m. It was confirmed that there is a maximum point of heat rejection at approximately $l_1/w_1 = 0.5$, regardless of the thickness of the fin. The region that satisfies a heat rejection of more than 100 W is $l_1/w_1 \leq 2.0$ for $d_F = 1$ mm and $l_1/w_1 \leq 4.0$ for $d_F = 2$ mm. When the fin thickness is 4 mm, the heat rejection always exceeds 100 W in the aspect ratio range $l_1/w_1 = 0.25$–4.00.

Table 2 summarizes the design parameters that, based on these parametric studies, best satisfy the requirements under consideration, that is, a heat rejection of more than 100 W, a specific heat rejection of more than 150 W/kg, and variation of radiator fin efficiency of more than 0.4.

C. Fabrication of the RTP

The RTP engineering model, which is a half-symmetry model, was fabricated based on the results of the parametric studies. Figure 8 shows the photos and images of the RTP EM. The RTP EM was composed of a base plate, heat transport units, surface material, insulation film, a thermal dummy, solar simulators, and a passive reversible rotary actuator. The materials and sizes of these items are listed in Table 3. A honeycomb sandwich panel was used as the base plate and 10 PGSs were used as the heat transport units, with 5 sheets being used as a radiator fin, and the other 5 as an absorber fin. Each PGS was attached with adhesive tape. Between the radiator fin and the absorber fin, embossed double-sided aluminized Mylar was installed for thermal insulation to the out-of-plane direction. Silverized polyester imide film (Ag/PEI) with a low α_S/ε_H value was attached for radiation on the surfaces of the honeycomb base plate and PGS radiator fin. No surface material was attached to the PGS absorber fin, because the PGS already has a high α_S/ε_H value.

A PGS thermal doubler, which forms part of the heat transport units, was placed between the honeycomb base plate and the thermal dummy. The thermal dummy, which was composed of a constantan wire heater attached to an A5052 plate, was bolted to the honeycomb base plate. The solar inputs were simulated by sheet heaters, which were attached to the absorber fin. The RTP prototype model was attached with positioning and clamping polycarbonate bolts to the A5052 support frame, which simulates the spacecraft interface during the test. Glass fiber spacers were placed between the RTP and the support frame. The support frame and the inner side of the base plate were covered with multilayer insulation (MLI).

Figure 9 shows the RRA-BBM, which consisted of an SMA torsion spring with a one-way memory effect, a bias spring, a bearing, a support cylinder, and an actuator housing. Before fabricating an RRA, several models of actuators, including a bimetal spiral spring and an SMA compression spring were designed and compared on weight and heat capacity. It was confirmed that the SMA torsion spring was the lightest and had the lowest heat capacity. Table 4 lists the specification of the SMA spring and the bias spring used in the RRA-BBM. The RRA-BBM was designed so that deployment starts when the SMA spring reaches its transformation temperature (approximately 10°C). When the SMA reaches its transformation temperature, it generates thermal torques that rotate the reversible fin toward its deployed position. As the temperature decreases, the torque of the bias spring becomes dominant and the actuator moves the fin toward its stowed position.

A flexible thermal strap consisting of 5 PGSs was installed between the thermal dummy plate and the RRA housing. Throughout the test, the actuator housing and flexible thermal strap were

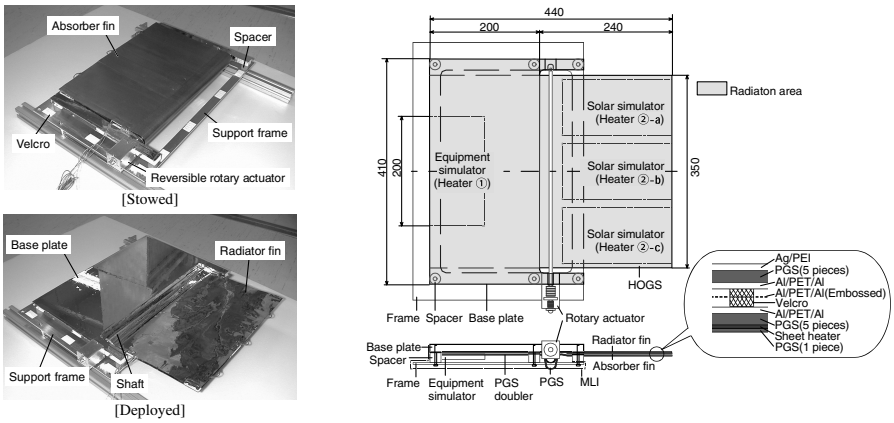

a) Photos of the RTP EM **b) Schematic of the RTP EM**

Fig. 8 RTP engineering model.

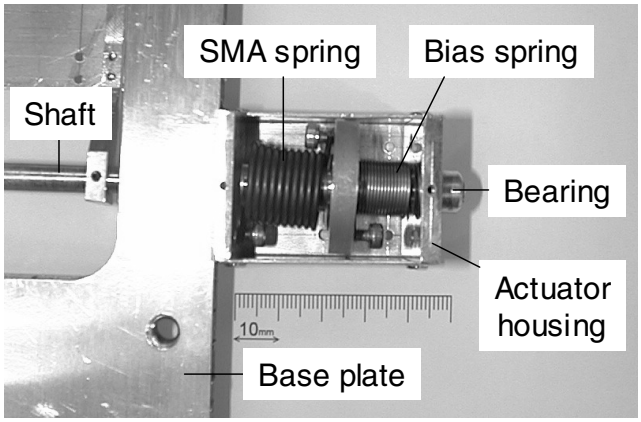

Fig. 9 Passive reversible rotary actuator.

thermally insulated by using MLI so that the RRA temperature corresponds only to the thermal dummy temperature.

IV. Thermal Test

A. Test System

Figure 10 shows the test system designed and constructed for the purposes of the present study. The system was composed of a thermal vacuum chamber, a measurement and power control unit, and a data acquisition system. The chamber had a cylindrical profile with its axis horizontal to the ground. The chamber size was 1.4 m in length and 0.8 m in inside diameter, and was equipped with a cold shroud wall, which was controlled to liquid nitrogen (LN2) temperature levels throughout the test. The shroud wall was coated with Chemglaze Z306 black paint with an emittance of approximately 0.90. Throughout the test, vacuum levels within the chamber were maintained at a pressure of 10^{-6} torr. The RTP was suspended by wires to minimize conduction heat loss from the chamber. The temperature distributions in the RTP were measured by 32 thermocouples (T-type, wire diameter of 200 μm). Additional thermocouples were used on the environmental sensors and the support equipment inside the chamber.

Table 4 Specifications of SMA springs and bias spring used in the reversible rotary actuator breadboard model.

	Characteristics	Values
SMA spring	Material	Ni-Ti-Co (54.5-44.0-1.5 %)
	Heat treatment time	500°C, 3 h
	Mass	5.8 g
	Wire diameter	1.5 mm
	Turns number	10
	Coil inner diameter	14 mm
	Length of moment arm	10 mm
Bias spring	Material	SUS 304
	Mass	1.7 g
	Young's modulus	186×103 N · mm
	Wire diameter	0.7 mm
	Turns number	15
	Coil inner diameter	11 mm
	Length of moment arm	10 mm

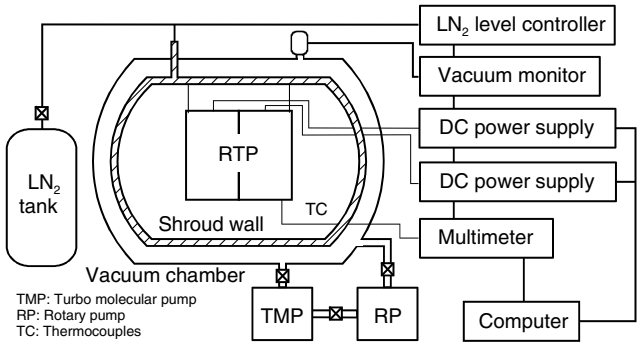

Fig. 10 Schematic of thermal vacuum chamber.

B. Test Program

The thermal vacuum tests of the RTP were divided into four types of tests: radiation retention tests, an absorption test, an autonomous thermal controllability test, and a power cycling test. The various test conditions are given in Table 5. The radiation retention tests were conducted to evaluate the heat-rejection capability of the RTP at arbitrary fin angles. In these tests, the RTP was not equipped with an RRA and was suspended horizontally in the chamber; the angle of the reversible fin was manually adjusted to 0, 45, 90, 135, and 180_deg by rotary motion feedthrough. The solar input simulation heaters were turned off, and the temperature of the thermal dummy was kept constant by a proportional-integral-differential (PID) control. The absorption test was conducted to evaluate the solar-absorption capability of the RTP when the reversible fin was stowed. In these tests, the RTP was not equipped with an RRA, and the reversible fin angle was adjusted to 0_deg (stowed position). The equipment simulation heater was turned off, and the solar simulation heaters were set to an input wattage of 10 W to 70 W. The autonomous thermal controllability test was conducted in order to evaluate changes in the heat-rejection capability accompanied by changes in the supplied heater power on the equipment simulator. In this test, the RRA was attached to the RTP, and the RTP was suspended vertically in the chamber to mitigate the effects of gravity. The solar input simulation heaters were turned off, and the thermal dummy heater was set to an input wattage of 5 W to 70 W. The power cycling test was conducted to evaluate the repeatability of the RTP autonomous control. In this test, the input wattage was changed between 20 W and 50 W. The temperatures of the RTP were recorded throughout the entire test at five-minute intervals. Each test was considered complete when the temperatures reached a steady state and changed by less than ± 0.5°C in 1 h.

C. Test Results and Discussions

1. Radiation Retention and Absorption Tests

Figure 11 shows the heat rejection of the RTP and the fin angles when the temperature of the thermal dummy was controlled at a constant −20, 20, and 60°C, respectively. The heat-rejection performances varied by a factor of more than 2.5 with changes in the fin angle from 0 to 180_deg. Table 6 shows the changes in heat rejection and radiator fin efficiency at fin positions between stowed and deployed. The maximum heat rejection of the RTP half-symmetry model was found to be 61.3 W. The radiator fin efficiency differences $\Delta\eta_F$ between the fin angles of 0 and 180_deg was 0.54, 0.45 and 0.39 when the temperatures of the thermal dummy were

Table 5 Test conditions.

Tests	RRA[a]	RTP setup	Fin angle	Thermal dummy	Solar input simulator
Radiation	Not equipped	Horizontal	0–180 deg	−20, 20, 60°C	0 W
Absorption	Not equipped	Horizontal	0_deg	0 W	10–70 W
Autonomous	Equipped	Vertical	Free	5–70 W	0 W
Cycling	Equipped	Vertical	Free	20 W/50 W	0 W

[a]RRA: Reversible rotary actuator

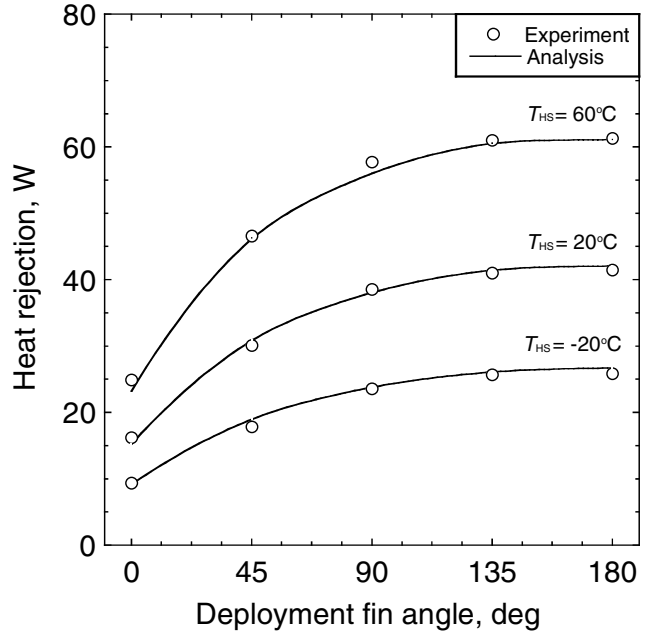

Fig. 11 Fin-angle dependences of the heat-rejection capability under equipment temperatures of −20, 20, and 60°C.

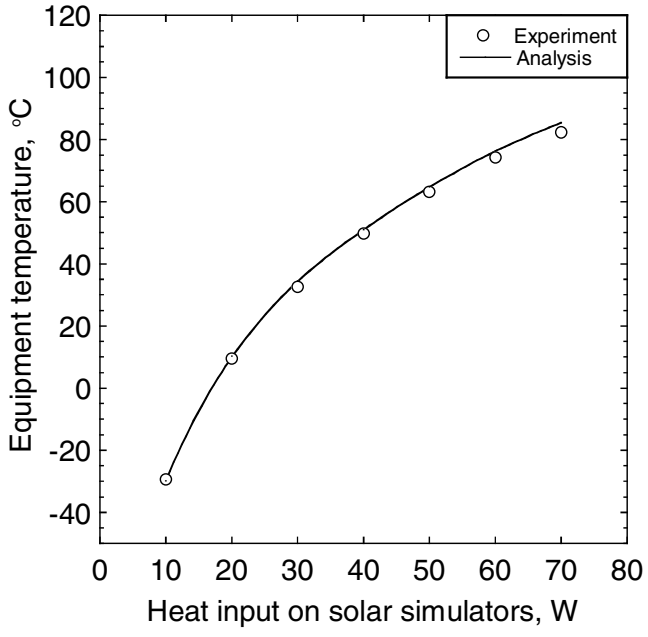

Fig. 12 Solar-absorption performance.

−20, 20, and 60°C, respectively. Table 7 shows the performance of the RTP evaluated from the radiation retention test results. The values of the maximum heat-rejection capability and specific heat rejection of the RTP EM were found to satisfy the design requirements discussed in the previous section. The value of the radiator fin efficiency change of the RTP did not meet the design requirement, although it was nearly equal to the required value ($\Delta\eta_F = 0.4$). This insufficiency is due to heat leaks between the base plate and stowed radiator fin, which could not be considered in the parametric studies.

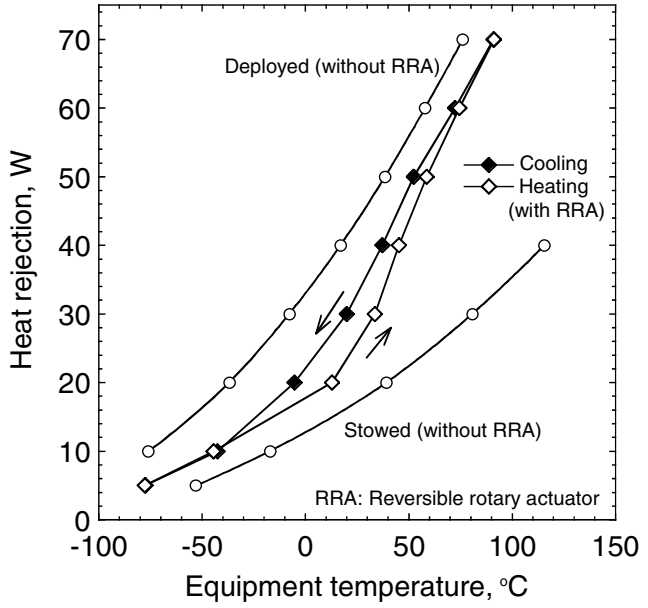

Fig. 13 Thermal controllability test result.

Figure 12 shows the relationship between the equilibrium temperature of the thermal dummy and the solar simulation heater power in the solar-absorption tests, along with the analytical results. The supplied power corresponded to the absorbed solar power around Mars, Earth, and Venus, as calculated from the solar intensities around these planets, the solar absorptance of the PGS, and the angles of solar incidence. These results confirm the efficacy of the solar-absorptive function of the RTP, because the temperature of the thermal dummy, which was turned off, was within the acceptable temperature range for general equipment. The thermal analyses in Figs. 11 and 12 were performed using SINDA to compare with the test results. As can be seen, the analytical and experimental results were in good agreement.

2. *Autonomous Controllability and Power Cycling Tests*

Figure 13 shows the test results of the autonomous test of the RTP with the RRA, with the performances when the fin angles were manually adjusted to 0 and 180_deg. It was confirmed that the heat-rejection performance of the RTP varied autonomously, although the radiator/absorber fin was not fully deployed/stowed due to insufficient deployment torque of the RRA-BBM. In comparing the cooling and heating processes, the presence of thermal hysteresis, which is a unique characteristic of the SMA, was also confirmed. To fully deploy and stow the reversible fins, it will be necessary to design an RRA with an SMA having higher deployment torque.

Figure 14 shows the temperatures of the front and back of the base plate, the tips of the radiator and absorber fins, and the MLI in the cycling test. It was confirmed that there were several bumps in the temperature change. At these points, the RRA was rotated along with the changes in temperatures, and, as a result, the sudden rises and falls of the equipment temperature were moderated. The test result also shows good repeatability within these five cycles, although a

Table 6 Heat rejection and radiator fin efficiency of the RTP engineering model.

	$\theta = 0$ deg		$\theta = 180$ deg		Difference		Ratio
Temperature	$Q_{\mathrm{RAD}(0\,\mathrm{deg})}$	$\eta_{F(0\,\mathrm{deg})}$	$Q_{\mathrm{RAD}(180\,\mathrm{deg})}$	$\eta_{F(180\,\mathrm{deg})}$	$Q_{\mathrm{RAD}(180-0\,\mathrm{deg})}$	$\Delta\eta_{F(180-0\,\mathrm{deg})}$	$Q_{\mathrm{RAD}(180\,\mathrm{deg})}/Q_{\mathrm{Rad}(0\,\mathrm{deg})}$
−20°C	9.35 W	0.30	25.8 W	0.83	16.5 W	0.54	2.8
20°C	16.2 W	0.28	41.5 W	0.73	25.3 W	0.45	2.6
60°C	24.9 W	0.26	61.3 W	0.64	36.4 W	0.39	2.5

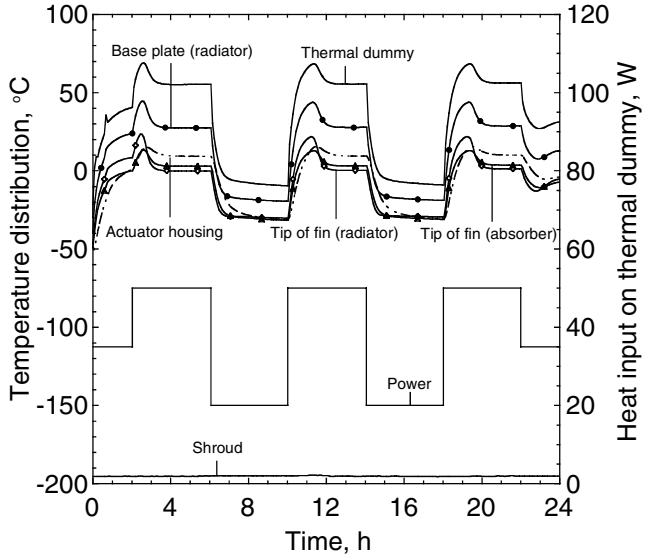

Fig. 14 Power cycling test result.

Table 7 RTP EM thermal performances.

Performance category	Required	Test results
Maximum heat rejection	>100 W	123 W
Specific heat rejection[a]	>150 W/kg	157 W/kg
Radiator efficiency change	>0.40	0.39

[a](Maximum heat rejection)/(RTP total weight)

thousand cycling tests are essential to evaluate the repeatability of the RRA strictly.

V. Conclusion

A new, passive, and lightweight 100 W-class deployable radiator with an environment-adaptive function in the form of an RTP was proposed, designed, and fabricated, and its thermal performance was evaluated by a series of thermal tests. The following results were obtained:

1) Parametric studies were conducted with detailed simulation models, and the RTP configuration that satisfies thermal requirements within the constraints of weight and fin efficiency variation was determined.

2) Based on our analytical results, an RTP engineering model was fabricated using high thermal-conductivity graphite sheets in the reversible fin, and a shape-memory alloy in the passive deployment/stowing actuator.

3) The radiation retention tests and absorption test without the RRA demonstrated that the RTP showed good specific thermal performance as both a radiator and as an absorber. The RTP showed excellent performance as a passive radiator from the standpoints of heat-rejection capability, specific heat rejection, and variation in the efficiency of the radiator fin. The effectiveness of the RTP as a solar absorber that can be substituted for a survival heater was also confirmed.

4) The autonomous thermal controllability test with the RRA-BBM demonstrated the variability of the thermal performance of the RTP, although full deployment and stowing of the reversible fin were not achieved by the RRA-BBM. For the future work, it will be necessary to design an RRA with an SMA having higher deployment torque.

The RTP in this paper has been considered as one of the thermal control devices for the Japanese Venus mission Planet-C, which will be launched in 2008, and an RTP preflight model has been under development since 2005.

Acknowledgement

This research was supported in part by the Japan Space Forum under the auspices of the Ground Research Announcement for Space Utilization Program and the Japan Society for the Promotion of Science.

References

[1] Lashley, C., Krein, S., and Barcomb, P., "Deployable Radiators—A Multidiscipline Approach," Society of Automotive Engineers, TP 98-1691, 1998.

[2] Goncharov, K., Orlov, A., Tarabrin, A., Gottero, M., Perotto, V., Tavera, S., and Zoppo, G. P.,"1500 W Deployable Radiator with Loop Heat Pipe," Society of Automotive Engineers, TP 2001-01-2194, 2001.

[3] Tachikawa, S., Ohnishi, Shimakawa, Y., Ochi, A., Okamoto, A., and Nakamura, Y., "Development of a Variable Emittance Radiator Based on a Perovskite Manganese Oxide," *Journal of Thermophysics and Heat Transfer*, Vol. 17, No. 2, 2003, pp. 264–268.

[4] Osiander, R., Champion, J. L., Darrin, A. M., Sniegowski, J. J., Rodgers, S. M., Douglas, D., and Swanson, T. D., "Micromachined Louver Arrays for Spacecraft Thermal Control Radiators," AIAA Paper 2001-0215, 2001.

[5] Braig, A., Meisel, T., Rothmund, W., and Braun, R., "Electro Emissive Devices—Progress Made in Development," Society of Automotive Engineers, TP 94-1465, 1994.

[6] Nagano, H., Tachikawa, S., and Ohnishi, A., "Passive and Active Thermal Control Devices—Variable Emittance Radiator and Reversible Control Panel," *4th Space and Astronautical Symposium*, Institute of Space and Astronautical Science, Sagamihara, Kanagawa, Japan, 2004, pp. 573–576.

[7] Ponnappan, R., Beam, J. E., and Mahefkey, E. T., "Conceptual Design of an 1 m Long `Roll Out Fin' Type Expandable Space Radiator," AIAA Paper 86-1323, 1984.

[8] Chow, L. C., and Mahefkey, E. T., "Fluid Recirculation, Deployment and Retraction of an Expandable Pulse Power Radiator," AIAA Paper 86-1322, 1984.

[9] Nagano, H., Ohnishi, A., Nagasaka, Y., and Nagashima, A., "Reversible Thermal Panel for Spacecraft Thermal Control (Evaluation of Effectiveness and Reliability of New Autonomous Thermal Control Device)," *Heat Transfer, Asian Research*, Vol. 34, No. 5, pp. 350–367, 2005.

[10] Nagano, H., Ohnishi, A., Nagasaka, Y., Mori, Y., and Nagashima, A., "Proton Irradiation Effects on Thermophysical Properties of High-Thermal-Conductive Graphite Sheet for Spacecraft Application," *International Journal of Thermophysics*, Vol. 27, No. 1, 2006, pp. 114–125.

[11] Nagano, H., Ohnishi, A., and Nagasaka, Y., "Thermophysical Properties of High-Thermal-Conductivity Graphite Sheets for Spacecraft Thermal Design," *Journal of Thermophysics and Heat Transfer*, Vol. 15, No. 3, pp. 347–353, 2001.

[12] Nagano, H., Kato, H., Ohnishi, A., and Nagasaka, Y., "Measurement of the Thermal Diffusivity of an Anisotropic Graphite Sheet Using a Laser-Heating AC Calorimetric Method," *International Journal of Thermophysics*, Vol. 22, No. 1, pp. 301–312, 2001.

[13] Gilmore, G., ed., *Spacecraft Thermal Control Handbook*, Aerospace Corp. Press, El Segundo, CA, 2002.